Catalysis Science & Technology

Accepted Manuscript

ROYAL SOCIETY OF CHEMISTRY

www.rsc.org/catalysis

Graphic abstract

g-C_3N_4 prepared from guanidine hydrochloride exhibited large surface area and the reduced recombination rates of electrons and holes, leading to the improved photocatalytic activity for degrading RhB under visible light.

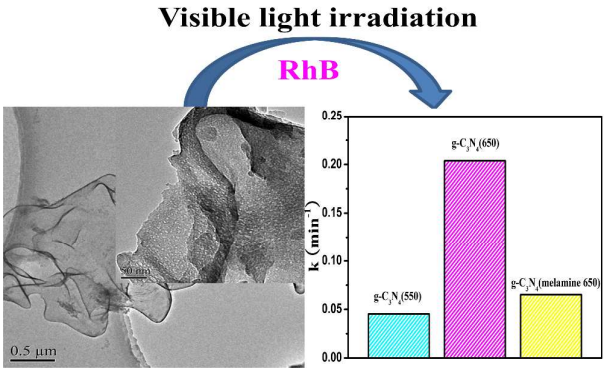

Polycondensation of guanidine hydrochloride into graphitic carbon nitride semiconductor with large surface area as visible light photocatalyst

Lei Shi [b], Lin Liang [a, c], Fangxiao Wang [b], Jun Ma [a] and Jianmin Sun [a, b*]

a: State Key Laboratory of Urban Water Resource and Environment, Harbin Institute of Technology, Harbin 150080, China

b: The Academy of Fundamental and Interdisciplinary Science, Harbin Institute of Technology, Harbin 150080, China

c: School of Life Science and Technology, Harbin Institute of Technology, Harbin 150080, China

*Corresponding author. Tel: +86 451 86403715;

E-mail address: sunjm@hit.edu.cn

Abstract

A low-cost, widely available and environmentally benign compound guanidine hydrochloride was applied to prepare g-C_3N_4 by thermal-induced polymerization at different temperature. The as-prepared g-C_3N_4 was thoroughly characterized by X-ray diffraction, Fourier transform infrared spectroscopy, elemental analyses, N_2 adsorption-desorption isotherms, thermal gravimetric analysis and differential scanning calorimetry, transmission electron microscopy, UV-vis diffuse reflectance spectra and photoluminescence spectra. It was noticeable that g-C_3N_4 prepared from guanidine hydrochloride possessed much larger surface area than that prepared from melamine. And its photocatalytic activity was evaluated by degrading Rhodamine B dye and demonstrated that the g-C_3N_4 synthesized from guanidine hydrochloride exhibited much higher activity than that prepared from melamine. Moreover, the activity can be further enhanced by increasing the condensation temperature of g-C_3N_4. In addition, the as-prepared g-C_3N_4 was also stable as demonstrated in the recycling experiments.

Keywords: guanidine hydrochloride, g-C_3N_4, visible light, RhB dye

1. Introduction

Semiconductor photocatalysis has drawn great attention due to its wide applications for hydrogen production from splitting water and degradation of environmental pollutants. [1-4] As the widely applied photocatalyst, TiO_2 has become the most studied material due to its high activity, stability and non-toxicity. [5, 6] However, the large band gap of TiO_2 (Eg=3.2 eV) and high recombination efficiency of photogenerated electron-hole pairs seriously limited its utilization of the solar spectrum. Therefore, the search for a low-cost, but stable and efficient visible light photocatalyst is highly desirable.

Recently, graphitic carbon nitride (g-C_3N_4) as visible light driven metal-free photocatalyst, was first reported by Wang et al. [7] With an optical band gap of 2.7 eV, g-C_3N_4 has been reported to possess excellent performance of hydrogen production from water splitting, [8-12] and degradation of organic pollutants under visible light irradiation. [13-18] Although g-C_3N_4 exhibited good activity and was easily prepared, the high recombination rates of the photogenerated electron-hole pairs and low surface area restricted its utilization of solar energy. Generally speaking, g-C_3N_4 was synthesized by thermal condensation of suitable precursors such as cyanamide, dicyandiamide, urea, thiourea, melamine, etc. [7, 19-22] A great many of strategies have been extensively employed to alter its electronic structure and texture so as to enhance its photocatalytic performance, including nonmetal or metal doping, [23, 24] coupling with semiconductor composite, [25-27] synthesizing mesoporous structures. [28-31] In order to better take advantage of g-C_3N_4, it is important to explore the novel strategy to synthesize large surface area g-C_3N_4 with cheap and eco-friendly substrate and further

improve its quantum efficiency.

It has been reported that the precursors containing the other elements besides the C, N and H elements would facilitate the thermal condensation process of g-C_3N_4 and enable structural alternation. Wang et al [32] reported that various guanidine compounds including guanidine thiocyanate, guanidine hydrochloride, guanidine carbonate were successfully used to synthesize g-C_3N_4. The g-C_3N_4 synthesized from guanidine thiocyanate exhibited a much higher H_2 evolution rate in water splitting than the reference sample prepared from dicyanamide. And the authors introduced that the resultant g-C_3N_4 from guanidine hydrochloride also exhibited comparable catalytic performance with g-C_3N_4 synthesized from guanidine thiocyanate. Lv et al [33] prepared carbon nitride quantum dots (g-CNQDs) by a facile one-step microwave-assisted approach with guanidine hydrochloride and EDTA as the precursors. As-prepared g-CNQDs exhibited chemiluminescence ability in the presence of NaClO. However, the systematic research on the g-C_3N_4 synthesis from guanidine hydrochloride was scarce. In this paper, g-C_3N_4 was synthesized from the low-cost, widely available and environmentally benign guanidine hydrochloride compound. It was found that the structure and photocatalytic activity of as-prepared g-C_3N_4 were very sensitive to polymerization temperature of precursor. Hence, the effects of polymerization temperature on the morphology and optical property of g-C_3N_4 materials were well investigated. Moreover, g-C_3N_4 synthesized from guanidine hydrochloride was used to photodegrade RhB dye under visible light, which possessed much higher photocatalytic activity than the reference sample

prepared from melamine. In addition, the photocatalytic activity of g-C_3N_4 increased with polymerization temperature, g-C_3N_4 polymerized at 650 °C displayed the optimum activity for degrading RhB.

2. Experimental

2.1 Sample preparation

The g-C_3N_4 photocatalyst was synthesized by the classic and facile method, which directly heating guanidine hydrochloride at different programmed temperatures under atmosphere. In detail, 4 g guanidine hydrochloride was placed in a crucible with a cover, and heated to the desired temperature for 3 h at a heating rate of 3 °C·min^{-1}. The resultant g-C_3N_4 samples were designated g-C_3N_4 (500), g-C_3N_4 (550), g-C_3N_4 (600) and g-C_3N_4 (650), respectively, according to different polymerization temperatures of 500, 550, 600 and 650 °C. For comparison, g-C_3N_4 was prepared from melamine by similar procedure. [22] 3 g of melamine was placed in a crucible with a cover, and heated to 500 °C for 2 h then 520 °C for 2 h at a heating rate of 4 °C·min^{-1} to obtain g-C_3N_4 (melamine 520). Moreover, the g-C_3N_4 was also prepared from melamine at 650 °C for 3 h to obtain g-C_3N_4 (melamine 650) as the reference sample.

2.2 Characterizations

The X-ray diffraction (XRD) measurement was carried out on Bruker D8 Advance X-ray powder diffractometer with Cu Kα radiation (40 kV, 40 mA) for phase identification. Fourier transform infrared spectroscopy (FTIR) was recorded within

400-4000 cm^{-1} on Perkin Elmer spectrum 100 using KBr discs. Elemental analyses (EA) for the carbon and nitrogen contents were performed on VarioMicro cube CHN analyzer. Thermal gravimetric analysis (TG) and differential scanning calorimetry (DSC) measurement were conducted using a Labsys Evo equipment (STA449C). The morphology and particle size of the products were examined by transmission electron microscopy (TEM, Tecnai G2 Spirit). N_2 adsorption-desorption isotherms were collected at 77 K using a Quantachrome NOVA 2000 surface area and porosity analyzer, samples were outgassed at 150 ℃ for 12 h prior to measurements. The UV-vis diffuse reflectance spectra (DRS) were measured on Perkin Elmer Lambda 750 UV-vis spectrometer. The photoluminescence spectra (PL) were obtained by a Varian Cary Eclipse spectrometer with an excitation wavelength of 325 nm at room temperature under atmosphere.

2.3 Photocatalytic test

The photocatalytic performance of g-C_3N_4 samples was evaluated through degradation of RhB. A 300 W Xe arc lamp provided visible light, and a glass filter was added to allow only visible light ($\lambda > 400$ nm) to pass through. 50 mg g-C_3N_4 sample was dispersed into 100 mL 5 $mg \cdot L^{-1}$ RhB solution under magnetic stirring. Prior to the light irradiation, the dispersion was kept in dark for 60 min under magnetic stirring to reach the adsorption-desorption equilibrium. Then solutions were collected every 5 min and centrifuged to remove the catalyst, then analyzed at 552 nm on UV-vis spectrometer. For comparison, the reactions were carried out in the presence of g-C_3N_4 (melamine) and in the absence of any catalyst. The efficiency of

degradation was calculated by C/C_0, where C is the concentration of remaining dye solution at each irradiated time interval, while C_0 is the initial concentration.

2.4 The stability of catalyst

The stability of g-C_3N_4 (650) under visible light irradiation was investigated by recycling experiments. After the photodegradation, the separated photocatalyst was washed with water and ethanol for several times, dried at 80 °C for 12 h, then applied to degrade a fresh 5 mg L^{-1} RhB aqueous solution under the same conditions for another run. The recycling process was repeated up to 5 times.

3. Results and Discussion

3.1 Characterization

Fig. 1 showed the XRD patterns of a series of resultant g-C_3N_4 samples. A typical g-C_3N_4 structure was detected, no other impurity phase was found. The main peaks at 27.3° and 13.0° were indexed to (002) and (100) planes of hexagonal g-C_3N_4 (JCPDS card no. 87-1526), corresponding to the graphite-like stacking and the in-plane structural repeating motifs of the conjugated aromatic units of g-C_3N_4. [19] With polymerized temperature increasing, the former peak of g-C_3N_4 shifted slightly from 27.3° to 27.8°, corresponding to a decrease in the interlayer stacking distance from 0.326 nm to 0.321 nm. This result implied that the stack of g-C_3N_4 became denser when guanidine hydrochloride was treated at higher temperature. The reduced layer distance revealed that the interlayer stacking order of resultant g-C_3N_4 was improved and its crystal structure tended to become more stable.[32] The intensity of the

other peak at 13.0° also increased with temperature, further proving the enhanced condensation at higher temperature. In addition, the additional peaks at 17.5 and 22.0° were formed in g-C_3N_4 (600) and g-C_3N_4 (650) samples, which were resulted from the denser packing or a distortion of melon structure in which every second melon sheet was displaced. [34, 35]

(Fig. 1)

Fig. 2 showed the FTIR spectra of a series of resultant g-C_3N_4. All the samples exhibited the typical IR patterns of graphitic carbon nitride. The broad bands in 3000-3500 cm^{-1} region could be attributed to the adsorbed O-H bands and N-H components. [30] The absorption peak at 809 cm^{-1} was considered as the out-of-plane skeletal bending modes of triazine. [29] The absorption bands in the range of 1200-1700 cm^{-1} were assigned to the typical stretching modes of C_3N_4 heterocycles. [28] The peaks at 1642 cm^{-1} were ascribed to C=N stretching vibration modes, while the 1242, 1320 and 1410 cm^{-1} attributed to aromatic C-N stretching vibration modes. And the intensities of stretching vibration peaks became stronger with condensation temperature increasing, suggesting g-C_3N_4 condensation was improved at higher temperature.

(Fig. 2)

To demonstrate the contents of various elements in resultant g-C_3N_4 samples, the elemental analyses were listed in Table 1. The atomic ratios of carbon to nitrogen in g-C_3N_4 at various temperatures were almost at 0.66, which were lower than 0.75 for the ideal g-C_3N_4 crystal. The hydrogen contents decreased with polymerization

temperature increasing, further suggesting the enhanced condensation with temperature. Incomplete condensation of g-C_3N_4 led to the residual hydrogen atoms bonding to the edges of the graphene-like C-N sheet in the form of C-NH_2 and 2C-NH bonds in amino groups. [13, 36, 37]

(Table 1)

The N_2 adsorption-desorption isotherms of the as-prepared g-C_3N_4 samples were displayed in Fig. 3A. All samples exhibited type IV isotherms except g-C_3N_4 (500), which were characteristic of mesoporous materials. Correspondingly, the BJH pore size distributions further confirmed the formation of mesopores. One was centered at 3-5 nm resulting from the existed mesopores in the layers, the other during 30-80 nm were associated with the accumulation of g-C_3N_4 layers. Table 2 summarized the texture properties of g-C_3N_4 samples. The surface area and pore volume of as-prepared g-C_3N_4 increased with treat temperature increasing, which were much larger than the reference samples prepared from melamine. The remarkably enhanced large surface area and pore volume were resulted from the drastic decomposition or volatilization of guanidine hydrochloride at higher temperature, which will be discussed in the following exploration of synthetic process for g-C_3N_4. The large surface area could supply more active species and the increased adsorption capacity to the dye, which might promote its photocatalytic activity.

(Table 2)

(Fig. 3)

In order to understand the phase transformation during the heating of guanidine

hydrochloride, the thermal analysis was carried out by TG-DSC. The detected temperature range was from room temperature to 900 °C at a heating rate of 10 °C·min^{-1}. An alumina crucible with a cover was used during thermal analysis to prevent sublimation of guanidine hydrochloride. The TG and DSC thermograms for guanidine hydrochloride clearly showed that in the semiclosed system several phase transformations were observed in Fig. 4A. The strongest peaks appeared in the temperature of 200-380 °C, contributed to 60% weight loss. During the temperature, two processes occurred. First, guanidine hydrochloride molecules polymerized into melamine by eliminating HCl and NH_3 from adjacent amino groups. Then melamine was transformed into melem below 380 °C. With the temperature increasing, two slight losses subsequently followed during 380-470 °C and 470-620 °C, the DSC thermogram also witnessed endothermic peaks. During the ranges, melem began polymerizing to form melon, then further forming g-C_3N_4, simultaneously amino groups went on further decomposing into NH_3, thus large amounts of bubbles were formed, which acted as the mesoporous templates, leading to the formation of mesoporous g-C_3N_4. According to the thermal analysis result, a possible synthetic process for g-C_3N_4 from guanidine hydrochloride was speculated in Scheme 1.

(Scheme 1)

(Fig. 4)

To further supply complete the evidence for Scheme 1, the FTIR and XRD characterizations of guanidine hydrochloride treated at different temperatures were performed. As the FTIR shown, compared with bare guanidine hydrochloride, when

guanidine hydrochloride was subjected to heat treatment at 380 °C, some stretching vibration peaks such as 522 cm^{-1}, 2150 cm^{-1} and 2760 cm^{-1} disappeared. The peak at 2150 cm^{-1} was ascribed to H-Cl stretching vibration mode, [38] and the disappearance of 2150 cm^{-1} implied that Cl was completely eliminated during the first step. With further heating at 500 °C, typical stretching vibration modes of g-C_3N_4 were exhibited. Furthermore, XRD patterns of guanidine hydrochloride treated at 380 °C were attributed to the melem-type compound. [39] At 500 °C, the existence peak at 27.3° suggested that the formation of g-C_3N_4.

Fig. 4 B shows the TG curve of g-C_3N_4 (550), it can be seen that almost no weight loss took place below 550 °C, however, the weight of the sample decreased rapidly between 600 and 700 °C, and discomposed totally at 700 °C, which indicated that g-C_3N_4 (550) could decompose and/or volatilize when the temperature was between 600 and 700 °C. The planar layer of g-C_3N_4 was cohered by the hydrogen bonding with NH/NH_2 groups between strands of polymeric melon units. Because the hydrogen bonding was not strong enough against thermal oxidation in air, the layer of aromatic CN unite could be gradually oxidized until vanished during thermal treatment. Combined with the TG-DSC curve and the yield result of g-C_3N_4 prepared at different temperature, it was inferred that the layer of g-C_3N_4 was possibly exfoliated by thermal oxidation at higher temperature. Similar reports about layer-exfoliating for the explanation of reduction in layer thickness at elevated temperature and/or prolonged time were also proposed. [40-42]

TEM images gave a direct insight into the morphology of the sample (Fig. 5). All

of resultant g-C_3N_4 displayed aggregated layers and irregular shapes. However, g-C_3N_4 (600) and g-C_3N_4 (650) displayed obvious worm-like porous structures as well as thinner nanosheets compared with g-C_3N_4 (500) and g-C_3N_4 (550). Porous structure and the large surface area of the photocatalyst would benefit to its activity. [42]

(Fig. 5)

The optical property of the resultant g-C_3N_4 samples was investigated by UV-vis diffuse reflectance spectroscopy in Fig. 6. All samples showed the typical absorption patterns with strong bandgap adsorption at about 460 nm, due to the excitation of electrons from the valance band to the conduction band of g-C_3N_4 semiconductor. Furthermore, their absorption edges were slightly affected by polymerization temperature. Correspondingly, the band gap energies of g-C_3N_4 (500), g-C_3N_4 (550), g-C_3N_4 (600) and g-C_3N_4 (650) were calculated at 2.75 eV, 2.70 eV, 2.83 eV and 2.88 eV, respectively. The band gap energy was reduced from 2.75 eV to 2.70 eV owing to the extension of electron delocalization in the aromatic sheets with enhanced structural condensation, somewhat similar to the red-shift effect in J-aggregates.[32] However, further increase of the temperature caused slight blue-shifts of the absorption edges, such as the band gap of g-C_3N_4 (600) increased to 2.83 eV, and 2.88 eV on g-C_3N_4 (650). The phenomena were attributed to the well-known quantum confinement effects induced by thinner (or smaller) nanosheets structure polymerized at higher temperatures. [21, 43]

(Fig. 6)

Since photoluminescence spectrum emission arises from the recombination of

excited electrons and holes, thus, PL technique is useful for disclosing the migration, transfer, and recombination processes of the photogenerated electron-hole pairs in the semiconductors. Fig. 7 exhibited the PL spectra of g-C_3N_4 samples, the PL spectra became broader and less intense with temperature increasing from 500 °C to 650 °C, which was possibly due to the restrained recombination of the photogenerated electrons and holes or the enhanced non-radiative recombination. The existence of mesopores and thinner layer in the g-C_3N_4 samples polymerized at higher temperature mainly facilitated the diffusion and transfer of electrons and thus leading to the fast separation of electrons and holes. [42, 44, 45]

(Fig. 7)

The photocatalytic capability of a series of g-C_3N_4 samples was evaluated by comparing the degradation efficiency for RhB under visible light. Prior to illumination, the adsorption of RhB on as-prepared g-C_3N_4 samples was carried out in the dark. As Fig. 8A shown, adsorption equilibrium was reached in 60 min for all the samples. The amounts of RhB adsorption on g-C_3N_4 (500) and g-C_3N_4 (melamine 520) were low at 4.9% and 2.0%. Adsorption amounts improved with increased BET surface areas of g-C_3N_4, and reached 14.6% for g-C_3N_4 (550), 17.2% for g-C_3N_4 (melamine 650), 26.8% for g-C_3N_4 (600) and 33.5% for g-C_3N_4 (650), respectively. After the adsorption reached equilibrium, the reaction system was irradiated by visible light. As presented in Fig. 8B, the degradation RhB hardly carried out even for 20 min without any catalyst. And the degradation efficiency of g-C_3N_4 (melamine 520) was also low at 10.2%. g-C_3N_4 (melamine 650) exhibited improved degradation efficiency

at 80%. For g-C_3N_4 samples prepared from guanidine hydrochloride, the degradation rates increased with the increments of the polymerization temperature. The g-C_3N_4 (650) showed the highest activity, almost 100% RhB was degraded in 20 min. Due to the larger surface area and existed mesopores or thinner layers on g-C_3N_4 (650), its photocatalytic activity was much higher than reference sample g-C_3N_4 (melamine 650). Fig. 8C illustrated the variations in optical absorption spectra of RhB with irradiation time over g-C_3N_4 (650). The obviously reduced absorption intensity indicated that RhB degraded completely after 20 min irradiation. A linear relationship between ln (C_0/C) and the irradiation time was shown in Fig. 8D. The linear relationships ($R \geq 0.99$) suggested that the photocatalytic degradation curves in all cases fit well with pseudo-first-order kinetics. Correspondingly, the degradation rate constants of various g-C_3N_4 samples were exhibited in Fig. 8E. The rate constants of g-C_3N_4 (500), g-C_3N_4 (550), g-C_3N_4 (600), g-C_3N_4 (650), g-C_3N_4 (melamine 520) and g-C_3N_4 (melamine 650) were 0.0118 min^{-1}, 0.0452 min^{-1}, 0.1250 min^{-1}, 0.2040 min^{-1} 0.0047 min^{-1} and 0.0652 min^{-1}. g-C_3N_4 (650) exhibited the highest rate constant, which was attributed to the larger surface area and the enhanced separation efficiency of photogenerated electron-hole pairs among the catalysts.

(Fig. 8)

The stability of a photocatalyst is important for the practical applications. Hence, the photocatalytic degradation experiments of RhB over g-C_3N_4 (650) were repeated up to five times under the same conditions and the results were shown in Fig. 9. It was evident that the photodegradation activity did not change markedly after five recycles,

which confirmed that g-C_3N_4 (650) was not photocorroded during the photodegradation process and kept good stability.

(Fig. 9)

In addition, the catalyst structure was further measured by FTIR and XRD after the five photodegradation runs. Fig. 10A showed that the FTIR of g-C_3N_4 (650) before and after the repeated reactions were almost the same as the fresh catalyst, suggesting the intact structure of catalyst. Similarly, the main peaks at 13.0° and 27.8° in XRD patterns did not change obviously, which further indicated that the catalyst structure was stable.

(Fig. 10)

4. Conclusions

g-C_3N_4 photocatalysts have been facilely prepared from cheap and environmentally benign guanidine hydrochloride at different polycondensation temperatures. The polycondensation temperature greatly affected the structure and catalytic activity of g-C_3N_4. The higher temperature at 650 °C was beneficial to the formation of mesoporous and thinner layer of g-C_3N_4, which resulted in the remarkably enhanced surface area and the reduced recombination rates of electrons and holes. These integrative positive factors led to the overall improved photocatalytic activity of g-C_3N_4 (650) for degrading RhB with visible light. It is hoped that our work opened a cheap and green synthetic process for g-C_3N_4 photocatalyst, which was promisingly applied in various fields.

Acknowledgement

We sincerely acknowledge the financial supports from National Natural Science Foundation of China (21373069), New Century Excellent Talents in University (NCET-10-0064), State Key Lab of Urban Water Resource and Environment of Harbin Institute of Technology (HIT2013TS01) and the Fundamental Research Funds for the Central Universities (HIT. IBRSEM. 201327).

References

1. E. S. Jang, J. H. Won, S. J. Hwang and J. H. Choy, Adv. Mater., 2006, **18**, 3309-3312.
2. R. Asahi, T. Morikawa, T. Ohwaki, K. Aoki and Y. Taga, Science, 2001, **293**, 269-271.
3. I. K. Konstantinou and T. A. Albanis, Appl. Catal. B: Environ., 2004, **49**, 1-14.
4. J. H. Park, S. Kim and A. J. Bard, Nano. lett., 2006, **6**, 24-28.
5. A. Fujishima and K. Honda, Nature, 1972, **238**, 37-38.
6. X. Chen, L. Liu, P. Y. Yu and S. S. Mao, Science, 2011, **331**, 746-750.
7. X. C. Wang, K. Maeda, A. Thomas, K. Takanabe, G. Xin, J. M. Carlsson, K. Domenet and M. Antonietti, Nat. Mater., 2009, **8**, 76-80.
8. A. Suryawanshi, P. Dhanasekaran, D. Mhamane, S. Kelkar, S. Patil, N. Gupta and S. Ogale, Int. J. Hydrogen. Energy, 2012, **37**, 9584-9589.
9. H. W. Kang, S. N. Lim, D. Song and S. B. Park, Int. J. Hydrogen. Energy, 2012, **37**, 11602-11610.

10. S. Martha, A. Nashim and K. M. Parida, J. Mater. Chem. A, 2013, **1**, 7816-7824.
11. H. Yan, Chem. Commun., 2012, **48**, 3430-3432.
12. Y. Wang, X. Wang and M. Antonietti, Angew. Chem. Int. Ed., 2012, **51**, 68-89.
13. L. Shi, L. Liang, J. Ma, F. Wang and J. M. Sun, Catal. Sci. Technol., 2014, **4**, 758-765.
14. Y. Yang, Y. Guo, F. Liu, X. Yuan, Y. Guo, S. Zhang, W. Guo and M. Huo, Appl. Catal. B: Environ., 2013, **142-143**, 828-837.
15. C. Pan, J. Xu, Y. Wang, D. Li and Y. Zhu, Adv. Funct. Mater., 2012, **22**, 1518-1524.
16. S. C. Yan, Z. S. Li and Z. G. Zou, Langmuir, 2010, **26**, 3894-3901.
17. S. Ye, L. G. Qiu, Y. P. Yuan, Y. J. Zhu, J. Xia and J. F. Zhu, J. Mater. Chem. A, 2013, **1**, 3008-3015.
18. J. Fu, Y. Tian, B. Chang, F. Xi and X. Dong, J. Mater. Chem., 2012, **22**, 21159-21166.
19. P. Niu. G, Liu and H. M. Cheng, J. Phys. Chem. C, 2012, **116**, 11013-11018.
20. F. Dong, L. Wu, Y. Sun, M. Fu, Z. Wu and S. C. Lee, J. Mater. Chem., 2011, **21**, 15171-15174.
21. G. Zhang, J. Zhang, M. Zhang and X. Wang, J. Mater. Chem., 2012, **22**, 8083-8091.
22. S. C. Yan, Z. S. Li and Z. G. Zou, Langmuir, 2009, **25**, 10397-10401.
23. G. Zhang, M. Zhang, X. Ye, X. Qiu, S. Lin and X. Wang, Adv. Mater., 2014, **26**, 805-809.
24. L. Ge, C. C. Han, J. Liu and Y. F. Li, Appl. Catal. A: Gen, 2011, **409-410**, 215-222.

25. S. Kumar, T. Surendar, A. Baruah and V. Shanker, J. Mater. Chem. A, 2013, **1**, 5333-5340.
26. X. Zhou, B. Jin, L. Li, F. Peng, H. Wang, H. Yu and Y. Fang, J. Mater. Chem., 2012, **22**, 17900-17905.
27. J. Sun, Y. Yuan, L. Qiu, X. Jiang, A. Xie, Y. Shen and J. Zhu, Dalton Trans., 2012, **41**, 6756-6763.
28. S. C. Lee, H. O. Lintang and L. Yuliati, Chem. Asian J., 2012, **7**, 2139-2144.
29. Y. Cui, J. Huang, X. Fu and X. Wang, Catal. Sci. Technol., 2012, **2**, 1396-1402.
30. J. Hong, X. Xia, Y. Wang and R. Xu, J. Mater. Chem., 2012, **22**, 15006-15012.
31. Y. Zhang, J. Liu, G. Wu and W. Chen, Nanoscale, 2012, **4**, 5300-5303.
32. B. Long, J. Lin and X. Wang, J. Mater. Chem. A, 2014, **2**, 2942-2951.
33. Y. Tang, Y. Su, N. Yang, L. Zhang and Y. Lv, Anal. Chem., 2014, doi: 10.1021/ac5005162.
34. D. Hollmann, M. Karnahl, S. Tschierlei, K. Kailasam, M. Schneider, J. Radnik, K. Grabow, U. Bentrup, H. Junge, M. Beller, S. Lochbrunner, A. Thomas and A. Brückner, Chem. Mater., 2014, **26**, 1727-1733.
35. T. Tyborski, C. Merschjann, S. Orthmann, F. Yang, M. C. Lux-Steiner and T. Schedel-Niedrig, J. Phys.: Condens. Matter., 2013, **25**, 395402-395408.
36. Y. Zhao, Z. Liu, W. Chu, L. Song, Z. Zhang, D. Yu, Y. Tian, S. Xie and L. Sun, Adv. Mater., 2008, **20**, 1777-1781.
37. L. Shi, L. Liang, J. Ma, F. Wang and J. M. Sun, Dalton Trans., 2014, **43**, 7236-7244.
38. K. Huang, J. Chen, C. F. Zhang, Z. H. Li, Q. H. Pan, Y. Sun, S. X. Liu, X. X. Liu, W. H. Li, Z. L. Yang, S. F. Weng, T. D. Hu, Y. Z. Xu and J. G. Wu, Sci China Ser B-Chem, 2009, **52**, 1825-1834.

39. B. Jürgens, E. Irran, J. Senker, P. Kroll, H. Müller and W. Schnick, J. Am. Chem. Soc., 2003, **125**, 10288-10300.

40. F. Dong, Z. Wang, Y. Sun, W. K. Ho and H. Zhang, J. Colloid Interf. Sci., 2013, **401**, 70-79.

41. F. Dong, M. Ou, Y. Jiang, S. Guo and Z. Wu, Ind. Eng. Chem. Res., 2014, **53**, 2318-2330.

42. P. Niu, L. Zhang, G Liu, and H. M. Cheng, Adv. Funct. Mater., 2012, **22**, 4763-4770.

43. A. P. Alivisatos, Science, 1996, **271**, 933-937.

44. X. Wang, S. Blechert and M. Antonietti, ACS Catal., 2012, **2**, 1596-1606.

45. X. Wang, K. Maeda, X. Chen, K. Takanabe, K. Domen, Y. Hou, X. Fu and M. Antonietti, J. Am. Chem. Soc., 2009, **131**, 1680-1681.

Figure Captions:

Fig. 1 XRD patterns of (a) g-C_3N_4 (500), (b) g-C_3N_4 (550), (c) g-C_3N_4 (600), and (d) g-C_3N_4 (650).

Fig. 2 FTIR spectra of (a) g-C_3N_4 (500), (b) g-C_3N_4 (550), (c) g-C_3N_4 (600), and (d) g-C_3N_4 (650).

Fig. 3 (A) N_2 adsorption-desorption isotherms and (B) BJH pore size distributions of (a) g-C_3N_4 (500), (b) g-C_3N_4 (550), (c) g-C_3N_4 (600), (d) g-C_3N_4 (650), (e) g-C_3N_4 (melamine 520) and (f) g-C_3N_4 (melamine 650). (Inset is enlarged pore size distributions up to 20 nm).

Scheme 1 Possible synthetic process from guanidine hydrochloride to g-C_3N_4.

Fig. 4 TG-DSC thermograms for (A) guanidine hydrochloride and (B) g-C_3N_4 (550), (C) FTIR and (D) XRD patterns of guanidine hydrochloride treated at different temperatures (a) 0 °C (b) 380 °C and (c) 500 °C.

Fig. 5 TEM images of (A) g-C_3N_4 (500), (B) g-C_3N_4 (550), (C) g-C_3N_4 (600), (D) - (E) g-C_3N_4 (650).

Fig. 6 UV-vis spectra of (a) g-C_3N_4 (500), (b) g-C_3N_4 (550), (c) g-C_3N_4 (600) and (d) g-C_3N_4 (650).

Fig. 7 Photoluminescence emission spectra of (a) g-C_3N_4 (500), (b) g-C_3N_4 (550), (c) g-C_3N_4 (600) and (d) g-C_3N_4 (650).

Fig. 8 (A) The adsorption curves of RhB; (B) Photodegradation curves of RhB; (C) UV-vis absorption spectra of RhB over g-C_3N_4 (650) for different irradiation time; (D) First-order kinetic plots for the photodegradation of RhB; (E) The rate constants of

various samples. (a) g-C_3N_4 (500), (b) g-C_3N_4 (550), (c) g-C_3N_4 (600), (d) g-C_3N_4 (650), (e) g-C_3N_4 (melamine 520), (f) g-C_3N_4 (melamine 650) and (g) without catalyst.

Fig. 9 Recycling runs in the photodegradation of RhB over g-C_3N_4 (650).

Fig. 10 (A) FTIR and (B) XRD patterns of g-C_3N_4 (650) before and after five recycling reactions.

Table 1 Different atom contents derived from EA analysis

Sample	N wt%	C wt%	H wt%	C/N atomic ratio
g-C_3N_4 (500)	60.16	33.97	1.90	0.66
g-C_3N_4 (550)	60.95	34.50	1.76	0.66
g-C_3N_4 (600)	61.52	34.98	1.59	0.66
g-C_3N_4 (650)	60.98	34.97	1.57	0.67
g-C_3N_4 (melamine 520)	34.45	62.02	2.05	0.65
g-C_3N_4 (melamine 650)	35.00	61.36	1.75	0.67

Table 2 Texture properties of various samples

Samples	Yield [a]	Surface area ($m^2 g^{-1}$)	Pore volume ($cm^3 g^{-1}$)	Pore size (nm)
g-C_3N_4 (500)	0.94	8.21	0.04	---
g-C_3N_4 (550)	0.79	16.08	0.09	3.69
g-C_3N_4 (600)	0.43	53.36	0.38	3.80
g-C_3N_4 (650)	0.13	65.08	0.52	3.95
g-C_3N_4 (melamine 520)	0.89	2.90	0.002	---
g-C_3N_4 (melamine 650)	0.33	19.00	0.15	2.14

a:The yield was obtained from 4 g guanidine hydrochloride or 3 g melamine three time average.

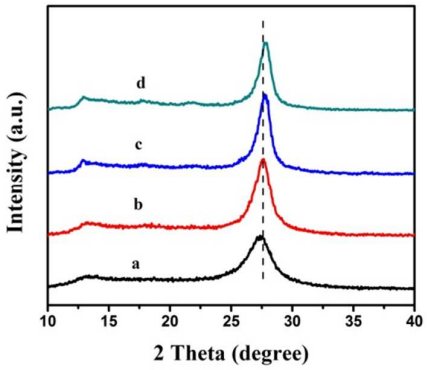

Fig. 1 XRD patterns of (a) g-C_3N_4 (500), (b) g-C_3N_4 (550), (c) g-C_3N_4 (600), and (d) g-C_3N_4 (650).

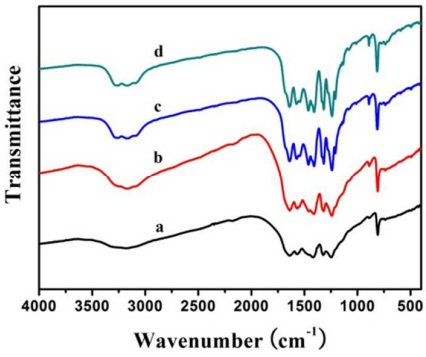

Fig. 2 FTIR spectra of (a) g-C_3N_4 (500), (b) g-C_3N_4 (550), (c) g-C_3N_4 (600) and (d) g-C_3N_4 (650).

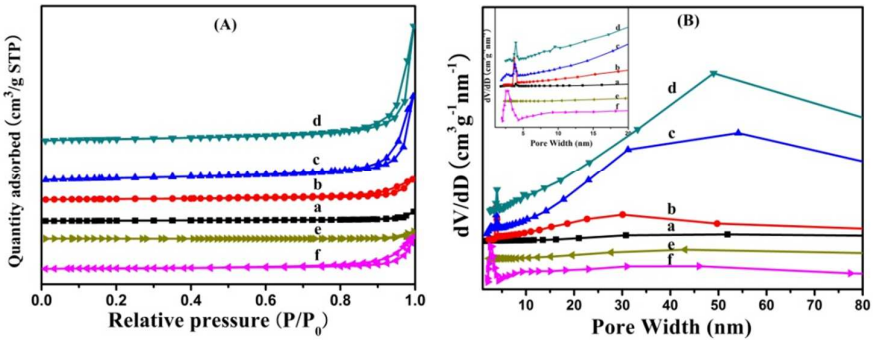

Fig. 3 (A) N_2 adsorption-desorption isotherms and (B) BJH pore size distributions of (a) g-C_3N_4 (500), (b) g-C_3N_4 (550), (c) g-C_3N_4 (600), (d) g-C_3N_4 (650), (e) g-C_3N_4 (melamine 520) and (f) g-C_3N_4 (melamine 650). (Inset is enlarged pore size distributions up to 20 nm).

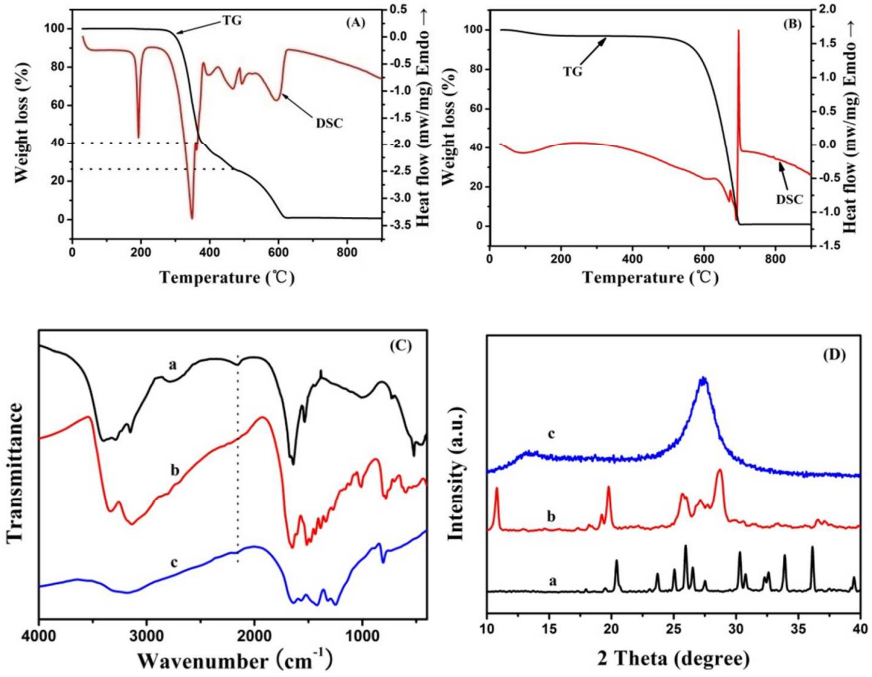

Fig. 4 TG-DSC thermograms for (A) guanidine hydrochloride and (B) g-C_3N_4 (550), (C) FTIR and (D) XRD patterns of guanidine hydrochloride treated at different temperatures (a) 0 °C (b) 380 °C and (c) 500 °C.

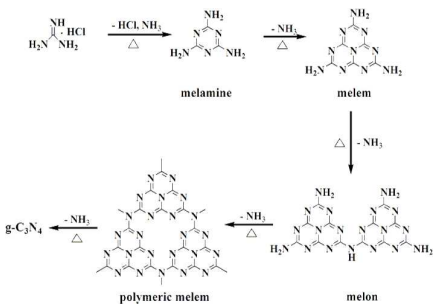

Scheme 1 Possible synthetic process from guanidine hydrochloride to g-C_3N_4.

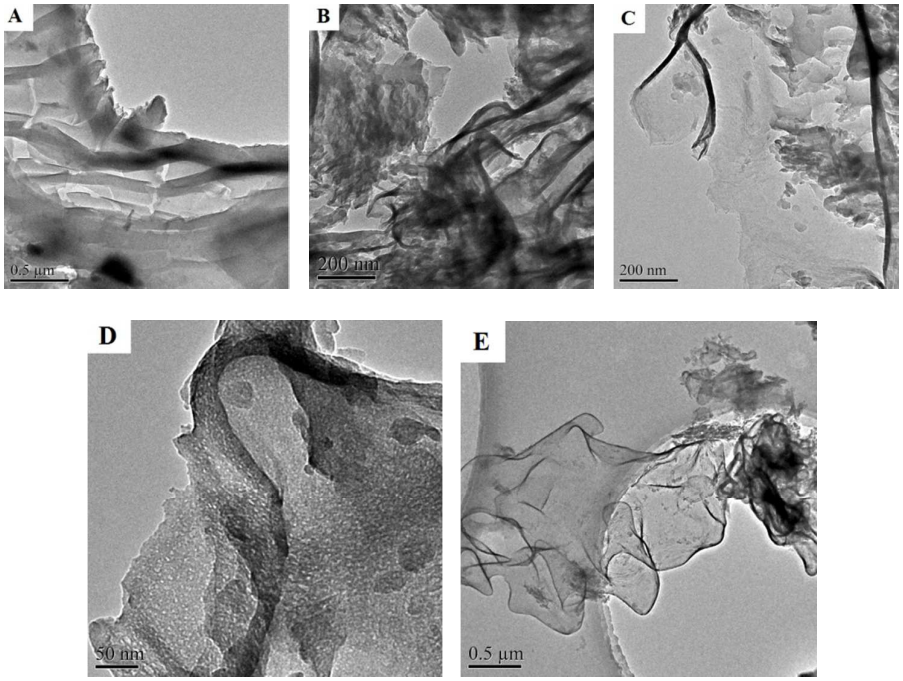

Fig. 5 TEM images of (A) g-C_3N_4 (500), (B) g-C_3N_4 (550), (C) g-C_3N_4 (600) and (D) -(E) g-C_3N_4 (650).

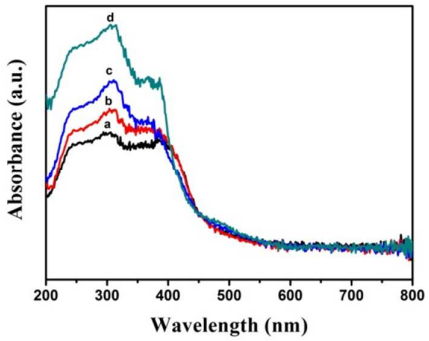

Fig. 6 UV-vis spectra of (a) g-C_3N_4 (500), (b) g-C_3N_4 (550), (c) g-C_3N_4 (600), and (d) g-C_3N_4 (650).

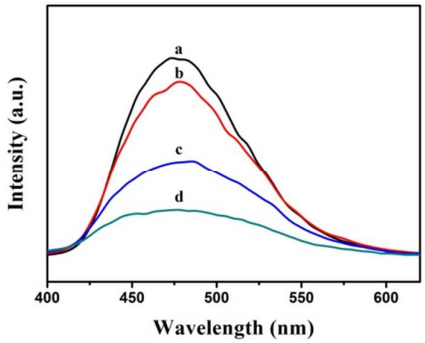

Fig. 7 Photoluminescence emission spectra of (a) g-C_3N_4 (500), (b) g-C_3N_4 (550), (c) g-C_3N_4 (600) and (d) g-C_3N_4 (650).

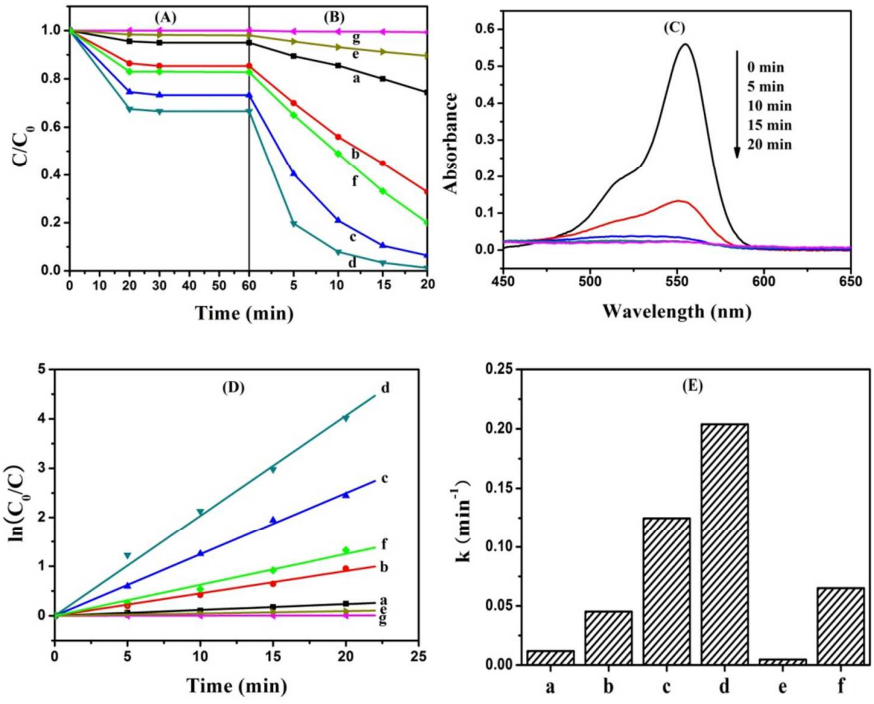

Fig. 8 (A) The adsorption curves of RhB; (B) Photodegradation curves of RhB; (C) UV-vis absorption spectra of RhB over g-C_3N_4 (650) for different irradiation time; (D) First-order kinetic plots for the photodegradation of RhB; (E) The rate constants of various samples. (a) g-C_3N_4 (500), (b) g-C_3N_4 (550), (c) g-C_3N_4 (600), (d) g-C_3N_4 (650), (e) g-C_3N_4 (melamine 520), (f) g-C_3N_4 (melamine 650) and (g) without catalyst.

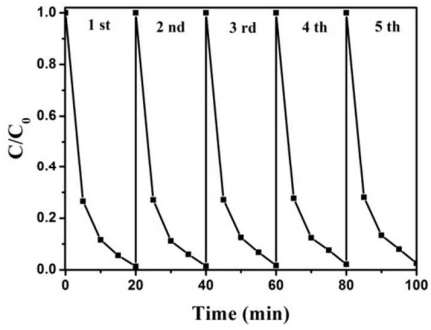

Fig. 9 Recycling runs in the photodegradation of RhB over g-C_3N_4 (650).

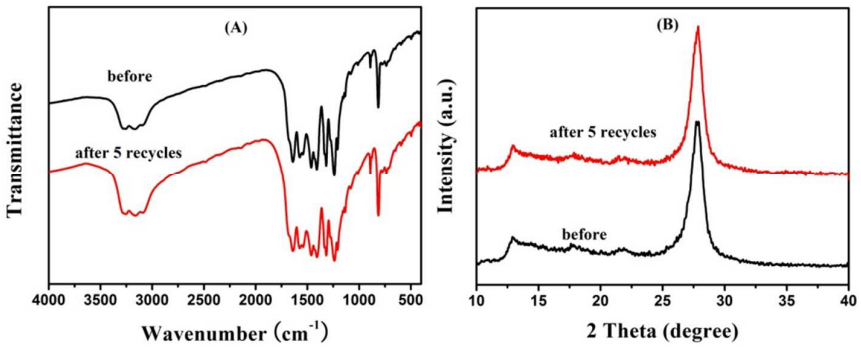

Fig. 10 (A) FTIR and (B) XRD patterns of g-C_3N_4 (650) before and after five recycling reactions.